Label swapper device for spectral amplitude coded optical packet networks monolithically integrated on InP

P. Muñoz,[1,*] **R. García-Olcina,**[2] **C. Habib,**[3] **L. R. Chen,**[3] **X. J. M. Leijtens,**[4] **T. de Vries,**[4] **D. Robbins,**[4] **and J. Capmany**[1]

[1]*Optical and Quantum Communications Group, Institute for Telecommunications and Multimedia Applications, Universitat Politècnica de València, c/ Camino de Vera s/n, 46022, Valencia, Spain*

[2]*Communications and Digital Systems Design Group, Electronic Engineering Department, Universitat de València, c/Vicent Andrés Estellés, s/n, 46100, Burjassot, Spain*

[3]*Photonics Systems Group, Electrical & Computer Engineering Department, McGill University, 3480 University Street, Montreal, Quebec H3A 2A7, Canada*

[4]*Opto-Electronic Devices group, Faculteit Electrical Engineering, Technische Universiteit Eindhoven, Postbus 513, 5600 MB Eindhoven, The Netherlands*

[*]*pmunoz@iteam.upv.es*

Abstract: In this paper the design, fabrication and experimental characterization of an spectral amplitude coded (SAC) optical label swapper monolithically integrated on Indium Phosphide (InP) is presented. The device has a footprint of 4.8x1.5 mm^2 and is able to perform label swapping operations required in SAC at a speed of 155 Mbps. The device was manufactured in InP using a multiple purpose generic integration scheme. Compared to previous SAC label swapper demonstrations, using discrete component assembly, this label swapper chip operates two order of magnitudes faster.

OCIS codes: (060.1155) All-optical networks; (060.4259) Networks, packet-switched; (130.4815) Optical switching devices; (130.6622) Subsystem integration and techniques; (250.5960) Semiconductor lasers; (130.7405) Wavelength conversion devices.

References and links

1. "Cisco visual networking index: forecast and methodology, 2009–2014," White Paper, Cisco Networks (2010).
2. S. J. B. Yoo, "Optical packet and burst switching technologies for the future photonic Internet," J. Lightwave Technol. **24**, 4468–4492 (2006).
3. R. Bolla, R. Bruschi, F. Davoli, and F. Cucchietti, "Energy efficiency in the future Internet: a survey of existing approaches and trends in energy-aware fixed network infrastructures," IEEE Commun. Surv. Tutorials **PP**, 1–22 (2010).
4. D. Blumenthal, B.-E. Olsson, G. Rossi, T. Dimmick, L. Rau, M. Masanovic, O. Lavrova, R. Doshi, O. Jerphagnon, J. Bowers, V. Kaman, L. Coldren, and J. Barton, "All-optical label swapping networks and technologies," J. Lightwave Technol. **18**, 2058–2075 (2000).
5. A. Srivatsa, H. de Waardt, M. Hill, G. Khoe, and H. Dorren, "All-optical serial header processing based on two-pulse correlation," Electron. Lett. **37**, 234–235 (2001).
6. P. Seddighian, J. Rosas-Fernández, S. Ayotte, L. Rusch, S. Larochelle, and A. Leon-Garcia, "Low-cost scalable optical packet switching networks with multi-wavelength labels," in *Proc. OFC/NFOEC* (2007), paper OthF5.
7. R. Gordon and L. Chen, "Demonstration of all-photonic spectral label-switching for optical MPLS networks," IEEE Photon. Technol. Lett. **18**, 586–588 (2006).
8. C. Habib, V. Baby, L. Chen, A. Delisle-Simard, and S. LaRochelle, "All-optical swapping of spectral amplitude code labels using nonlinear media and semiconductor fiber ring lasers," IEEE J. Sel. Top. Quantum Electron. **14**, 879–888 (2008).

9. C. Cole, B. Huebner, and J. Johnson, "Photonic integration for high-volume, low-cost applications," IEEE Commun. Mag. **47**, S16–S22 (2009).
10. E. Bente and M. Smit, "Ultrafast InP optical integrated circuits," in *Optoelectronic Integrated Circuits VIII*, L.A. Eldada and E.-H. Lee, eds., Proc. SPIE **6124**, 612419 (2006).
11. X. Leijtens, "JePPIX: the platform for InP-based photonics," in *Proceedings of the 15th European Conference on Integrated Optics* (ECIO, 2010), pp. ThG3–1/2.
12. N. Calabretta, J. Hyun-Do, J. Llorente, E. Tangdiongga, T. Koonen, and H. Dorren, "All-optical label swapping of scalable in-band address labels and 160-Gb/s data packets," J. Lightwave Technol. **27**, 214–223 (2009).
13. J. den Besten, "Integration of multiwavelength lasers with fast electro-optical modulators," Ph.D. thesis, TU Eindhoven (2004).
14. B. Saleh and M. Teich, *Fundamentals of Photonics* (Wiley, 2007), Chap. 2.
15. M. Smit and C. Van Dam, "PHASAR-based WDM-devices: principles, design and applications," IEEE J. Sel. Top. Quantum Electron. **2**, 236–250 (1996).
16. G. Eisenstein, "Semiconductor Optical Amplifiers," IEEE Circuits Devices Mag. **5**, 25–30 (1989).
17. P. Munñoz, R. Garcia-Olcina, J. D. Domenech, M. Rius, J. Capmany, L. R. Chen, C. Habib, X. J. M. Leijtens, T. de Vries, M. R. Heck, L. M. Augustin, R. Nötzel, and D. J. Robbins, "Multi-wavelength lasers based on an arrayed waveguide grating and Sagnac loop reflectors monolithically integrated on InP," in *Proceedings of the 15th European Conference on Integrated Optics* (ECIO, 2010), pp. WeF2–1/2.
18. P. Munoz, D. Pastor, and J. Capmany, "Modeling and design of arrayed waveguide gratings," J. Lightwave Technol. **20**, 661–674 (2002).
19. L. Soldano and E. Pennings, "Optical multi-mode interference devices based on self-imaging: principles and applications," J. Lightwave Technol. **13**, 615–627 (1995).
20. Y. Barbarin, E. Bente, T. de Vries, J. den Besten, P. van Veldhoven, M. Sander-Jochem, E. Smalbrugge, F. van Otten, E. Geluk, M. Heck, X. Leijtens, J. van der Tol, F. Karouta, Y. Oei, R. Notzel, and M. Smit, "Butt-joint interfaces in InP/InGaAsP waveguides with very low reflectivity and low loss," in *Proc. Symposium IEEE/LEOS Benelux Chapter,* (IEEE, 2005).
21. C. E. Spurgeon, *Ethernet: The Definitive Guide* (O'Reilly & Associates, Inc., 2000).
22. A. Zilkie, J. Meier, M. Mojahedi, P. Poole, P. Barrios, D. Poitras, T. Rotter, C. Yang, A. Stintz, K. Malloy, P. Smith, and J. Aitchison, "Carrier dynamics of quantum-dot, quantum-dash, and quantum-well semiconductor optical amplifiers operating at 1.55 μm," IEEE J. Quantum Electron. **43**, 982–991 (2007).
23. F. Soares, F. Karouta, E. Geluk, J. Zantvoort, H. de Waardt, R. Baets, and M. Smit, "Low-loss InP-based spot-size converter based on a vertical taper," in *Proceedings of the 15th European Conference on Integrated Optics* (ECIO, 2005), pp. 104–107.
24. R. Garcia-Olcina, "Sistema de fabricacion de altas prestaciones de redes de difraccion de Bragg en fibra y aplicaciones al campo de los sensores opticos y a los sistemas de comunicaciones opticas," Ph.D. thesis, Universitat Politecnica Valencia (2008).

1. Introduction

The traffic conveyed in data networks has grown steadily over the last two decades, and growth of 30 to 60 Peta Byte (PB) per month from 2011 to 2014 are forecasted [1]. The core transmission infrastructure is mainly optical, but connection oriented. Thus, packet switching in optical networks has been subject of research, seeking for flexibility and network efficiency over traditional circuit-switched networks [2]. More specifically, optical code multi-protocol label switching (OC-MPLS) promises fast, flexible, power-efficient switching by keeping signals in the optical domain and avoiding costly conversions to the electrical domain [3]. In optical packet-switching technology each packet is identified by a specific label with local significance on each network switch. A local label look-up table, built at the beginning of the communication, is used to determine the output path for the packet, according to the input label and port to the switch. A new label is then assigned to the packet, of use in the next network switch. Although there are a significant number of techniques [2] for the implementation of optical label swapping, the mainstream research has focused in three of them, Sub-Carrier Multiplexed (SCM) labels [4], time domain multiplexing (TDM), or serial labels [5] and Spectral Amplitude Coded (SAC) labels [6]. The third technique, combines the advantages of both SCM and TDM labels: the payload and label are concurrent in time and have the same duration, as in SCM labels, but they are separated far apart in the wavelength spectrum and can have different rate. To be more precise, each bit on the label is represented by a single wavelength. So a reserved set
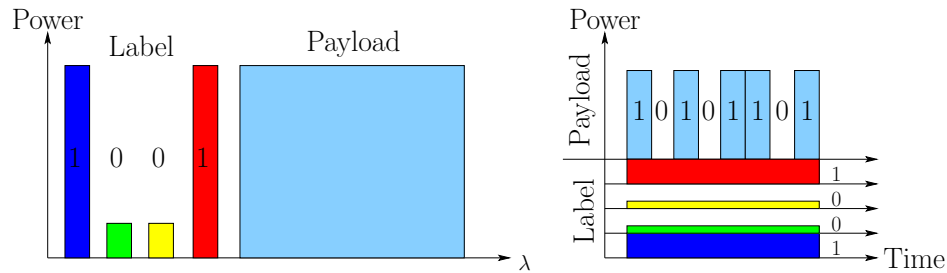
Fig. 1. Spectral Amplitude Coded (SAC) label time and wavelength domain representations.

of wavelengths, is allocated for the coding of the label, N wavelength slots, therefore enabling 2^N-1 labels (discounting the all-zero label). This is shown in Fig. 1.

All in all, the label is a number represented by a stream of bits (which are represented in wavelength). Swapping labels means changing the state of some or all the bits. Thus, the optical implementation requires the ability to perform several digital logic operations in the optic domain, in particular NAND and NOR gating. In SAC labeling this translates into being able to perform these operations on a per wavelength basis at a few hundred Mbps. SAC swapping devices using cross-gain modulation (XGM) in ring cavities have previously been demonstrated with high extinction and contrast ratios [7]. In particular, a proof-of-concept tabletop ($2x1$ m^2) label-swapper using a two stage XGM-based fiber-ring laser has been demonstrated in [8]. The main drawbacks of this device were cost and low operating frequency (80 kHz) due to a lengthy cavity (8.9 m). In [12] a different SAC label swapper implementation using a Semiconductor Optical Amplifier-Mach Zehnder Interferometer (SOA-MZI) was demonstrated at a label rate of 4 MHz, according to the packet payload duration (256 ns, payload rate 160 Gbps). Both SAC swapping devices were constructed by assembling a large number of discrete components. A practical cost-effective implementation requires small footprint in the form of photonic integrated circuits [9]. We thus present, a photonic integrated circuit that performs parallel per-wavelength digital logic operations required in a SAC label swapping node. The circuit is monolithically integrated in Indium Phosphide (InP) technology [10], using a multiple purpose generic integration scheme [11], hence compatible with state of the art commercial components for optical communications. The circuit operation speed is two orders of magnitude higher than in [12], with a footprint five orders of magnitude smaller, than the previously reported equivalent subsystems [8].

This paper is structured as follows: in section 2, the design of the device is described. Section 3 is devoted to the description of two operation modes, with focus on the results. Hence, and for clarity on the device operation, the details on the experiments, and on the fabrication technology are provided separately in section 4. Finally, the conclusions are drawn in section 5.

2. Device design

The device is based on a linear multi-wavelength laser configuration [13], built using several Sagnac Loop Reflectors (SLR) [14], one Arrayed Waveguide Grating (AWG) [15] and several Semiconductor Optical Amplifiers (SOAs) [16] on a single InP chip. A micro-graph of the device is provided in Fig. 2-(a) [17]. The device is a linear laser between the SLRs enclosing SOA$_2$-AWG-SOA L$_i$ i=1...4, where the SOA$_2$ acts a common cavity gain medium, and the AWG and SOA L$_i$ combination enable the different output wavelengths/labels. The light is out-coupled from the laser cavity using a side diffraction order of the AWG [18], denoted 'FSR out
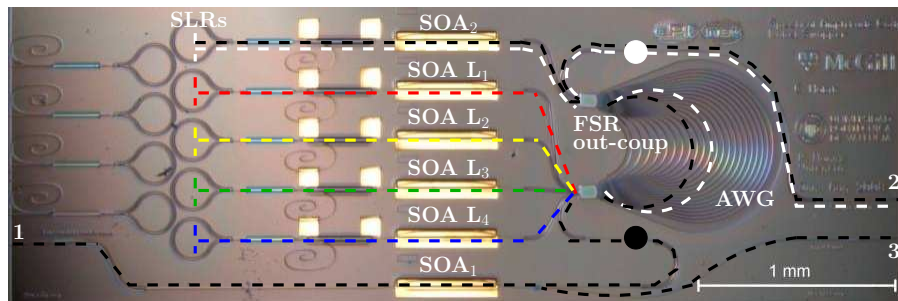
(a) Label Swapper (LS) chip micro graph
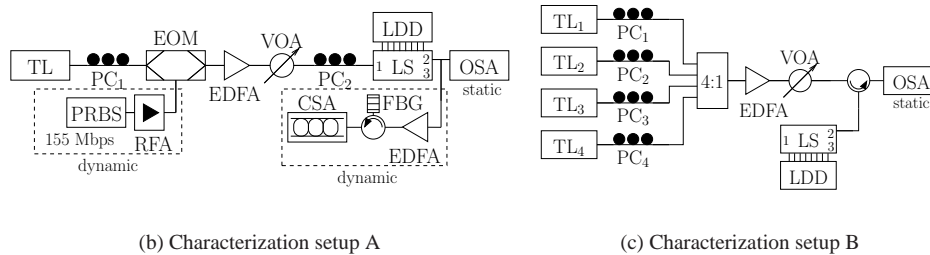
(b) Characterization setup A

(c) Characterization setup B

Fig. 2. Device micro graph, inputs/outputs 1, 2, 3 and SOA's labeled (a) and characterization setups (b)(c) (TL Tunable Laser, PC Polarization Controller, EOM Electro-Optic Modulator, RFA Radio-Frequency Amplifier, PRBS Pseudo Random Bit Sequence generator, EDFA Erbium Doped Fiber Amplifier, VOA Variable Optical Attenuator, LS Label Swapper chip, LDD Laser Diode Driver, OSA Optical Spectrum Analyzer, FBG Fiber Bragg Grating, CSA Communications Signal Analyzer).

coup' in the figure, through the waveguide named '2' in the figure. An additional waveguide, denoted '1', at the SOA L_i side is laid out as input for the incoming labels, through SOA_1 that can be used as pre-amplifier. This waveguide extends also directly to the right hand side of the chip -by mean of a coupler-, denoted '3' in the figure, and it is used for complimentary purposes (reference, alignment and control).

The AWG was designed to work at λ_0=1550 nm, with 2 input and 5 output spectral channels spaced $\Delta\lambda_c$= 1.6 nm. The design is for a cyclic response, FSR=5*1.6=8 nm, and for two diffraction orders [18] to be available at the input/output slab couplers. Hence 50:50 out coupling from the laser cavity can be performed without the need of an additional power splitter, since input waveguides have the same spectral transfer function, as labeled in Fig. 2-(a) as 'FSR out-coup'. The loop reflectors are Sagnac interferometers with a 2x2 MMI coupler [19] that provides a $\pi/2$ phase shift between the two outputs, necessary for total reflection [14]. Although just one waveguide in the Sagnac is used, the other one is terminated in a pigtail/spiral shaped waveguide, Fig. 2-(a), to minimize unwanted reflections due to possible imperfections. The SOA sections have a length of 500 μm. The amplifiers SOA_2 and SOA's L_i, i=1..4, are used to obtain sufficient gain for lasing to occur at each cavity. Additionally, thermo-optic heaters are laid between the SOAs and the Sagnacs, to control the cavity phase. The designed Fabry-Perot cavity length between SLRs is 6.7 mm, which is the determinant feature in the operation speed.

3. Device characterization

3.1. Overview

Without the event of incoming signals to the swapper, the device works as a regular multi-wavelength laser [13]. However, when incoming signals/labels are used as inputs, with proper wavelengths, the device lasing operation can be optically controlled. In particular, if the input signals are encoded in amplitude, logical operations can be performed.

Two sets of experiments were conducted, both with similar equipment detailed in Fig. 2-(b) and (c). Each experiment demonstrates a different operation mode. The first operation mode, described in section 3.2, demonstrates swapping from one input wavelength to one or many, but simultaneous, output wavelengths. The second operation mode, section 3.3, shows the operation from a set of input to a set of output wavelengths, with pairs of input/output wavelength operating independently.

In both experiments, tunable lasers (TL) were used to provide the input signals. Variable Optical Attenuators (VOAs) were employed to set their power levels to the appropriate operating point on the device input vs. output power static transfer function, with the TLs being operated in Continuous Wave (CW) mode. The static operation curves were obtained from the peaks measured in the traces acquired by means of an Optical Spectrum Analyzer (OSA). In the first set of experiments based on the setup illustrated in Fig. 2-(b), the maximum operational speed, i.e., the label rate, was assessed by using the additional hardware shown within dashed boxes. A pseudo-random bit sequence (PRBS) generator provided the digital pulses, Non-Return to Zero (NRZ), to modulate the amplitude of the CW TLs by means of an Electro-Optical Modulator (EOM). A Communications Signal Analyzer (CSA) was then used to measure the quality factor (Q) of the signal returned from the chip.

3.2. Single input wavelength operation

The device was operated using waveguides '1' and '2' as input and output respectively, as detailed in Fig. 2-(b). Referring also to Fig. 2-(a), the output lasing wavelengths were enabled at '2' by biasing SOA_2 and SOAs L_i (dashed white and color lines). Next, an external laser signal with proper wavelength to reach SOA_2 through the AWG was used as input in '1' (dashed black line). The SOAs biases were adjusted to allow switching on and off the on chip lasing by turning off and on the input, so the output is an inverted version of the input.

The single input to single output static transfer function curves are shown in Fig. 3-(a). The traces are shown in the same colors as the ones used to mark the lasing cavities in Fig. 2-(a). The graphs and caption detail how the input signal is translated in wavelength and inverted in amplitude to the output. Moreover, the input signal was modulated with a PRBS generator operated at 155 Mbps. This operation rate is 2 orders of magnitude higher than similar SAC label swapping experiments reported with non-integrated devices (4 Mbps) [12], hence allowing for higher label rates and/or shorter guard times (i.e., less overhead). The quality factor of the converted digital signal is shown in Fig. 3-(b). The insets provide screen-shots of the digital eye patterns at the marked operation points in the static curves, b_1, b_2 and b_3. Quality factors greater than 6, corresponding to a bit error rate (BER) smaller than 10^{-9}, were attained. The extinction ratio measured back to back for the equivalent average power was between 10 and 11 dB for an average power in [-6,-3] dBm. In this range, the measured extinction ratio for SOAs L1 to L4 was in [4,14] dB, [2,4] dB, [2,6] dB and [4,13] dB respectively.

The operation was also tested with the PRBS operated at 622 Mbps, as shown in the dashed inset within Fig. 3-(b). Though significant bit patterning effects can be observed due to the carrier recovery time associate with these particular SOAs, Q factors greater than 6 were still obtained.
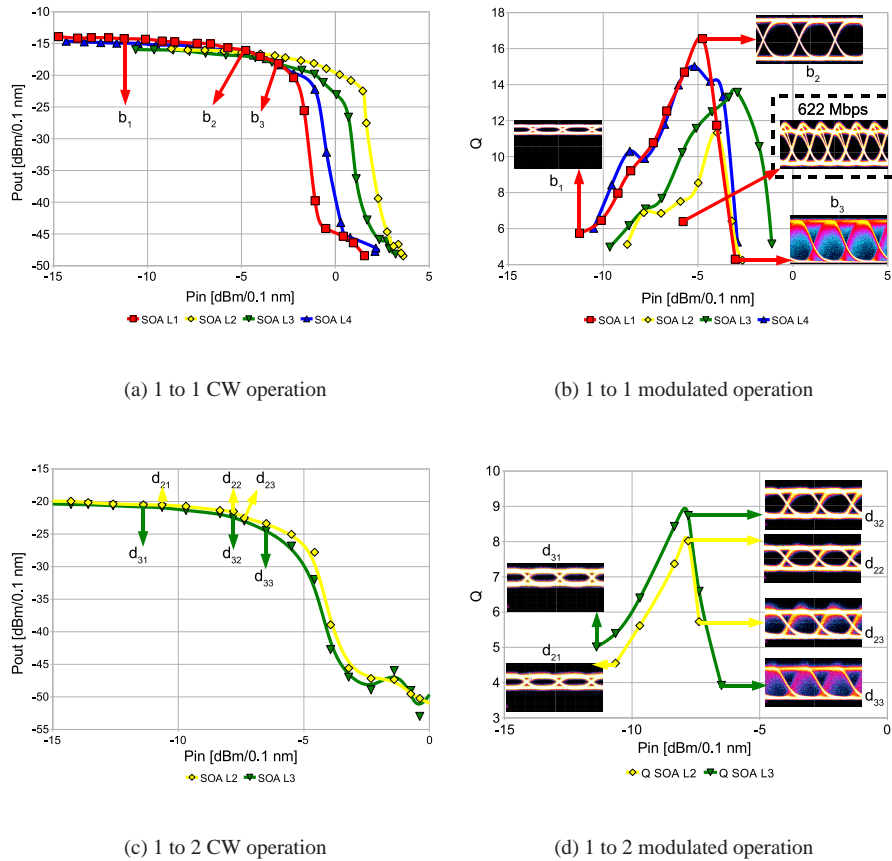
(a) 1 to 1 CW operation

(b) 1 to 1 modulated operation

(c) 1 to 2 CW operation

(d) 1 to 2 modulated operation

Fig. 3. Experimental results with setup A, Fig. 2-(b). Input through chip input '1' at wavelength 1561.8 nm, chip output '2' at wavelengths for SOA L_i i=1,2,3,4: 1576.30 nm, 1574.61 nm, 1573.01 nm and 1571.32 nm respectively. The colors correspond to those of Fig. 2-(a). Sub-figures (a) and (b) represent the static (CW in/out) and dynamic (modulated in/out) operation of the device, whilst (c) and (d) represent the static and dynamic operation for one input and two simultaneous outputs. The insets in the dynamic traces (b) and (d) are the eye pattern diagrams (155 Mbps if otherwise not indicated), for which the operation point is correspondingly marked in the static curves (a) and (c). All the power values refer to on-chip average power.

A single input can also be mapped to several outputs. The static and dynamic (155 Mbps) results, are shown in Fig. 3-(c) and (d) respectively, when two outputs are enabled at the same time. This can be of use when one input bit is used to reset or set more than one output bit. The results are only presented for two simultaneous outputs. In the configuration of Fig. 2-(b) it is also possible to enable the four wavelengths at the same time. However, as detailed in [17], for the four lasers to have wavelengths within the same AWG FSR, the needed bias currents were as high as to disallow on/off switching with the input wavelength/label. This might be solved in forthcoming designs by improving the overall architecture to minimize waveguide propagation, device insertion and fiber in/out coupling losses. Moreover, mode-hopping between the AWG side modes takes place in this particular device when more than two wavelengths are used. This disallows dynamic operation, as a filter is employed before the BER analyzer. The mode hopping can also be prevented using more aggressive designs for the AWG, i.e. with narrower channel bandwidth and larger FSR [13].

3.3. Parallel input wavelength operation

The device is also able to operate on a per wavelength basis, meaning each input wavelength controls one output wavelength. This is a per-bit, or parallel, operation. In this case, as detailed in Fig. 2-(c), waveguide '2' was used as input and output. An optical circulator was required to inject and collect the light to/from the chip with a single fiber. Hence, each input wavelength reaches one of the SOAs L_i, instead of the common SOA_2 as in the previous case. Therefore individual per wavelength parallel operation is possible.

Referring also to Fig. 2-(a), all the output lasing wavelengths were enabled by biasing SOA_2 and all the SOAs L_i. The static input vs. output transfer function curves are shown in Fig. 4-(a). The inset shows also two OSA traces corresponding to the curves' starting and ending points (input on/output off and input off/output on). The input wavelengths are marked with arrows. The output wavelengths are marked with the same symbols as in the curves. Colors are used to show the relations between input and output wavelength. Some examples of 4 bit to 4 bit conversion are shown in Fig. 4-(b), (c) and (d). Some satellite peaks appear between the input and output wavelength sets, due to imperfect side diffraction order lasing in the device [13], but their peak power is always at least 20 dB less than the output wavelengths. No dynamic operation measurements were made for this configuration, as results are expected to be similar to those of the previous setup.

4. Materials and methods

4.1. Experiment details

The device was soldered to a copper chuck and its temperature was kept at 25 C during the measurements by means of a Peltier cell. The the chuck holder was water-cooled to dissipate the heat produced by the current injection in the active areas of the chip. A multi-contact wedge was used to probe the SOA's, and a lensed fiber was aligned with the output waveguide using a nano-positioning stage. Prior to any system measurement, the FP cavity length was confirmed by measuring the multi-wavelength laser spectra with a 10 pm resolution OSA. The FP mode spacing resulted in 51.4 pm, corresponding to the cavity length of 6.7 mm with an average group index of 3.5. The waveguide losses (5 dB/cm) and lensed fiber in/out coupling losses (6 dB) were measured through test structures. The AWG insertion loss was 8.5 dB. The waveguides in the arms of the AWG were designed as deeply etched [10] of 1.5 μm width, aiming at matching TE and TM effective indexes. The SOAs structure provides gain for TE polarization.

In setup A, Fig. 2-(b), the external light source was a tunable laser model IQS-2400 from EXFO, emitting +8 dBm at 1561.81 nm. This wavelength corresponds to one of the AWG pass bands, therefore it can pass through the AWG and reach the SOA_2, Fig. 2-(a). The polarization

(a) 4 to 4 CW operation

(b) 1101 to 0010 conversion
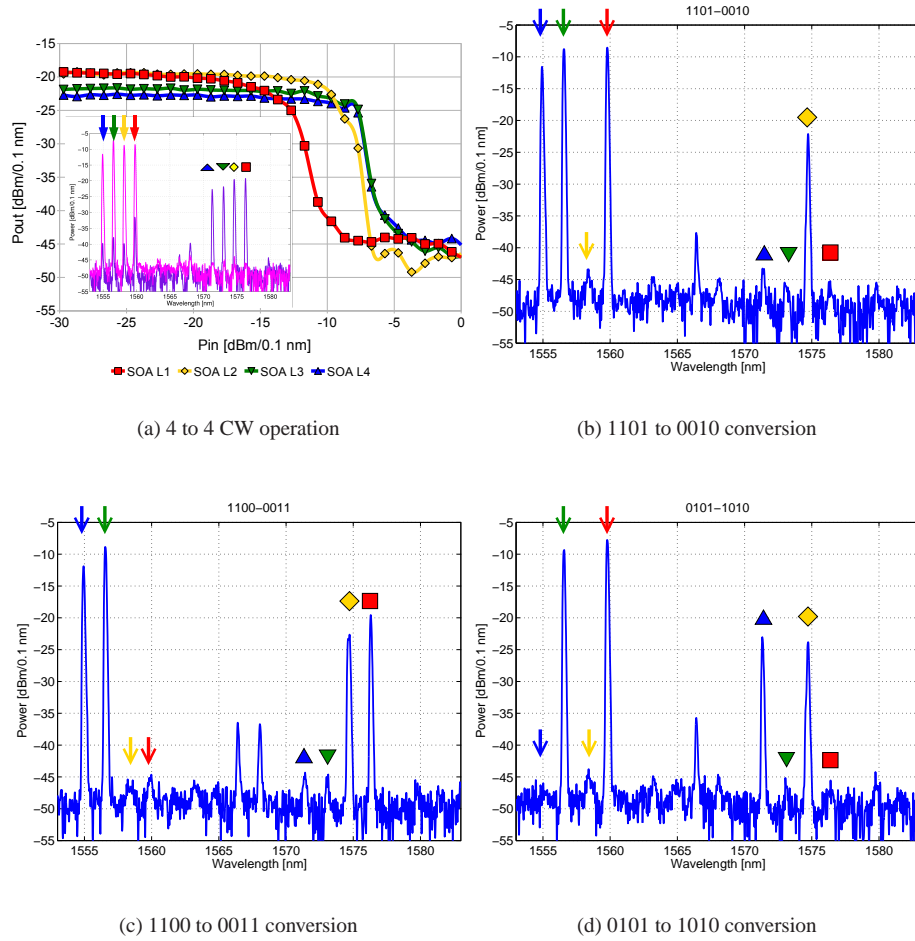
(c) 1100 to 0011 conversion

(d) 0101 to 1010 conversion

Fig. 4. Experimental results with setup B, Fig. 2-(c). The input wavelengths to SOA L$_i$, i=1,2,3 and 4 are, respectively: 1559.77 nm, 1558.13 nm, 1556.58 nm and 1554.94 nm, output wavelengths as in setup A. The colors correspond to those of Fig. 2-(a). Sub-figure (a) presents the 4 input to 4 output CW operation, and the inset OSA traces correspond to P$_{in}$ = - 30 dBm/0.1 nm/channel -magenta- and P$_{in}$ = 0 dBm/0.1 nm/channel -pink-. OSA traces (b)(c) and (d) show different 4 bit input/output combinations. Markers on the OSA traces match those of the figure. Arrows for the input wavelengths are used, each in the color corresponding to their associated output. All the power values refer to on-chip average power.

of the external laser light was rotated before feeding the electro-optical modulator from Avanex (up to 10 Gbps) by means of a manual polarization controller from Fiberpro, in order to maximize the modulation efficiency. The modulator was driven by a 155 Mbps PRBS digital signal coming from a SONET/SDH test module model OTS9100 from Tektronix, and amplified by an RF electrical amplifier model SA1137 from WJ Communications. For the static curves, the electrical amplifier was powered off, so the external laser signal was not digitally modulated.

The external laser signal was amplified 20 dB by a fixed-gain EDFA from Accelink Technologies, and a variable optical attenuator based on MEMS technology, model VP1-30 from Sercalo, was used to vary the on-chip input power, with attenuation from 0 to 35 dB. The optical properties of the integrated SOAs showed a strong dependence on the polarization state of the input signal, so an additional polarization controller was used before the chip input in order to align the polarization state of the external laser signal and the polarization state of the spontaneous emission from the SOA_2. The polarization alignment was performed by means of an Lightwave Polarization Analyzer model 8509C from Agilent. To set up the proper point of operation, SOAs L_i and SOA_2 were contacted by electric probes and electrically biased by means of a Laser Diode Driver model PRO8000 from Thorlabs, in a such way that the internal L_i lasers were switched between on and off states when the external signal from EXFO laser was injected in the chip. The electrical current values for '1 to 1 CW operation', Fig. 3-(a), were: I_{L1} = 40 mA and I_{SOA2} = 28.2 mA for λ_1; I_{L2} = 28 mA and I_{SOA2} = 32 mA for λ_2; I_{L3} = 27 mA and I_{SOA2} = 28 mA for λ_3; I_{L4} = 34 mA and I_{SOA2} = 28 mA for λ_4. I_{SOA1} = 100 mA was keep constant for all the wavelengths. The electrical current values for '1 to 2 CW operation', Fig. 3-(c), were: I_{L2} = 28.1 mA, I_{L3} = 26.1 mA, I_{SOA2} = 29.3 mA and I_{SOA1} = 100 mA. Due to the cross gain modulation (XGM) effect in SOA_2, when external laser was enabled the SOA_2 gain was saturated and that caused that internal laser L_i was switched off, and vice versa.

For the static measurements, the output signal from '2', Fig. 2-(a), was measured using a Optical Spectrum Analyzer (OSA) from HP model 70951A with a resolution of 0.1 nm. The static curves, Fig. 3-(a), were obtained by varying the on-chip input power by means of the VOA and acquiring the peak data by a custom software developed in LabVIEW™.

To obtain the dynamic curves, the electrical amplifier was switched on and fed with a digital signal at 155 Mbps from the PRBS generator. A fiber Bragg grating (FBG) designed and fabricated in the Optical and Quantum Communications Group (OQCG) facilities at the Universidad Politecnica de Valencia, was connected at the chip output in reflective configuration, and mechanically tuned in order to isolate the wavelength of interest while filtering out the ASE noise from the EDFA. The grating was fabricated irradiating intrinsically photosensitive fiber PS1250/1500 from Fibercore™with a 500 μm wide spot of 244 nm UV light and using a novel FBG fabrication technique developed at the OQCG [24]. By this technique a 5-cm long Gaussian apodized FBG was fabricated employing a single 1 cm long uniform phase mask from Ibsen Photonics™. The peak refractive index variation was of 7e-5, producing an spectral response with a transmission at peak wavelength of -18 dB, and a 3 dB-bandwidth of 0.1 nm. The single-wavelength digitally modulated optical signal was then characterized by a Communication Signal Analyzer model DSA8200 from Tektronix, and different signal quality parameters, as Q factor, were obtained.

In setup B, Fig. 2-(c), the external light sources were four tunable lasers model IQS-2400 from EXFO, emitting +10 dBm at 1554.94 nm, 1556.58 m, 1558.13 nm and 1559.77 nm, respectively. The light was injected and collected by the port '2' using an optical circulator. These wavelengths correspond again to the AWG pass bands, therefore the four external signals can pass through the AWG and reach the four corresponding SOAs L_i, Fig. 2-(a). As mentioned before, the optical properties of the integrated SOAs showed a strong dependence on the polarization state of the input signal, so the polarization of the external lasers were individually

rotated before being combined by a passive 4x1 coupler by means of four manual polarization controllers, in order to align the polarization state of each external laser signals and the polarization state of the spontaneous emission from their corresponding SOA L_i. No additional polarization controller was used before the chip, but high care in stabilizing fiber pigtails and connection on the optical table was taken.

The 4 combined external laser signals were amplified 20 dB by an fixed-gain EDFA from Accelink Technologies, and a variable optical attenuator based on MEMS technology, model VP1-30 from Sercalo, was used to vary the on-chip input power, attenuation range from 0 to 35 dB.

To set up the proper operation point, the SOAs L_i and SOA_2 were contacted by electric probes and electrically biased in such a way that the internal L_i lasers switched between on and off states when the corresponding external signals from EXFO lasers were injected in the chip. Note that in this case the XGM effect takes place in every individual SOA L_i instead of in SOA_2 as in setup A, so the electrical currents for the proper operation were different. The electrical current values in this case were $I_{L1} = 36.9$ mA, $I_{L2} = 28.1$ mA, $I_{L3} = 25.4$ mA, $I_{L4} = 28.5$ mA and $I_{SOA2} = 30$ mA. The SOA_1 was not used in this configuration. Due to the XGM effect in each SOA L_i, when the corresponding external lasers were enabled the SOA L_i gain was saturated and that caused that internal laser L_i was switched off, and vice versa.

4.2. Fabrication details

The label-swapper device has been fabricated using an integration technology based on InP/InGaAsP. This technology is able to produce integrated optical circuits that can contain devices built up from active and passive waveguide elements. The passive waveguides can be low contrast (shallowly etched) waveguides or high contrast (deeply etched) waveguides. Both types can be realized on the same chip using Reactive Ion Etching [13] and several masking steps. By using a suitable doping profile in the top layers and applying a metal contact on the top of the passive waveguide an electro-optic phase modulator can be realized [13]. Due to the fact that in this semiconductor system both the refractive indexes (> 3) and the contrast are high, the light is tightly confined and therefore the radius of curvature of curved waveguides can be small. In our design, the minimum radius of curvature of deeply etched passive waveguides was limited to 100 μm, so a relatively complex subsystem, such as this label-swapper, which includes several components (one AWG, five Sagnac mirrors, six SOAs and 3 input/output waveguides) has a footprint as small as 4.8×1.5 mm^2.

Additionally, active devices such as optical amplifiers and saturable absorbers can be realized in predefined areas which have an active layer stack on the chip. These active areas are made using a selective area regrowth technique. The layers are grown by Metal-Organic Vapour Phase Epitaxy (MOVPE) with all metal-organic precursors in a three-step process. In the first epitaxy step, a 500 nm thick active film is grown, that provides optical confinement and gain. This film consists of 190 nm quaternary InGaAsP material (Q1.25, $\lambda_{bandgap} = 1.25$ μm), a 120 nm Q1.55 layer providing the gain, and a 190 nm Q1.25 layer. In addition, the first 200 nm p-doped InP top cladding layer is grown. A SiN$_x$ mask layer is deposited by Plasma-Enhanced Chemical Vapour Deposition (PECVD) and patterns of active regions that are 30 μm wide with a length ranging from 20 to 2000 μm are defined by photolithography and etched into the SiN$_x$. Outside the masked regions, the layers are removed down to the first Q1.25 layer, with a combination of dry and wet etching that leaves an overhang in the SiN$_x$ mask. Then a 500 nm thick passive undoped Q1.25 waveguide layer and a 200 nm undoped InP cladding is selectively grown outside the masked regions. The overhang in the mask ensures a flat surface and a low-loss butt-joint between the active and passive areas. Subsequently, the SiN$_x$ mask is removed and a common 1300 nm thick, p-doped InP top layer with gradually increasing doping level is

grown on both the passive and active regions, with a highly p-doped ternary InGaAs contact layer on top. Local planarisation with polyimide is used that also provides passivation of the active waveguide. A Ti-Pt-Au metallisation scheme is applied, which was selected because it provides low-resistance ohmic contacts to both the p-doped InGaAs and the n-doped InP layers.

Shallowly etched active waveguides are fabricated in the active layer regions. The analysis of sub-threshold spectra of extended cavity lasers shows that reflections of transitions from the passive to the active (amplifying) areas in shallow waveguides at the butt-joint interface can be kept at −50 dB or less [20]. This is particularly relevant for this label-swapper subsystem since feedback above −50 dB can seriously affect the behavior of the laser system.

5. Discussion and conclusion

A photonic chip, of application in SAC label swapping, and produced monolithically in InP technology, has been presented in this paper. Compared to previous demonstrations using discrete component assembly, the device footprint is greatly reduced and the operation speed for label processing is increased by more than two orders of magnitude. Scalability in wavelength is possible by using larger port count AWGs. Combination with other building blocks to perform complimentary functions, for instance to spectrally separate the payload and intermediate swapping wavelengths, is possible by means of the generic integration technology described.

One important aspect for the label swapper is the on/off device response. As mentioned before, this is related to the rate at which packets occur, i.e., the label rate in SAC label swapping. The advantage of SAC label swapping is the label is decoupled from the payload in the wavelength domain, hence they may have significantly different rates. For instance, a payload length of 64 bytes, (minimum length for an Ethernet frame [21]), at a payload rate of 160 Gbps [12], translates to a packet rate (equivalent to label rate in SAC label swapping) of less than 320 Mpbs. The results in this paper show complete operation at 155 Mbps as well as the possibility for operation at 622 Mbps. The limitation in this current design is mainly due to the SOAs carrier recovery. The SOAs are based on a Multi-Quantum Well structure (MQW, see 'Methods'), and other researchers have shown that Quantum-Dot (QD) SOAs can perform at least 6 times faster than MQW ones [22].

Other important issue is the optical power balance, which is to be improved, as on chip power at the input/output. This figure can be improved (less input power required to switch, more output power) for instance by means of spot size converters, for a more efficient light in/out coupling (0.5 dB at [23]), and/or by including an additional integrated SOA as booster amplifier for the output signal.

Finally, besides the particular and relevant application of the device demonstrated in this paper, the concept and functionality can serve other purposes. In general, the device can be operated as logical NAND or NOR gate through wavelength conversion, but at very modest rate (hundreds of Mbps) compared to other photonic integrated converters based on SOA-MZI, that can be found in the literature elsewhere.